Aqueous ionic and complementary zwitterionic soluble surfactants: Molecular dynamics simulations and sum frequency generation spectroscopy of the surfaces

*Michal Petrov, Babak Minofar, Luboš Vrbka, and Pavel Jungwirth**

Institute of Organic Chemistry and Biochemistry, Academy of Sciences of the Czech Republic and Center for Biomolecules and Complex Molecular Systems, Flemingovo nám. 2, 16610 Prague 6, Czech Republic

Patrick Kölsch[#] and Hubert Motschmann*

Max-Planck Institute of Colloids and Interfaces, Am Mühlenberg 2, 14476 Golm, Germany

[#]*Present address: University of Leipzig, Faculty of Physics and Earth Science, Linnestrasse 5, 04103 Leipzig, Germany*

**Corresponding authors. E-mails: pavel.jungwirth@uochb.cas.cz (P. J.) and koelsch@physik.uni-leipzig.de (P. K.)*

Abstract

An aqueous ionic surfactant 1-dodecyl-4-dimethylaminopyridinium (DMP) bromide and the corresponding zwitterion 2-(4-dimethylaminopyridinio)-dodecanoate (DPN) were explored by means of molecular dynamics (MD) simulations and, for the ionic system, by infrared-visible sum frequency generation (IR-VIS SFG). The molecular structure of the interfacial layer was investigated for the ionic and zwitterionic systems as a function of surfactant concentration, both in water and in salt (KF or KBr) solutions, by MD simulations in a slab geometry. The build up of the surface monolayer and a sublayer was monitored, and density and orientational profiles of the surfactants were evaluated. The difference between the ionic and zwitterionic systems and the effect of the added salt were analyzed at a molecular level. The results of MD simulations were compared to those of nonlinear optical spectroscopy measurements. Infrared visible sum frequency generation (IR-VIS SFG) was employed to study the DMP ionic surfactant in water and upon addition of simple salts. The influence of added salts on the different molecular moieties at the interface was quantified in detail experimentally.

Introduction

Amphiphilic species, such as ionic or zwitterionic surfactants tend to form a two dimensional film at the air/water interface. This behavior is described in thermodynamic terms of surface tension and surface excess. The basic description is given by the Gibbs adsorption isotherm[1] $d\gamma = -\Gamma\, d\mu$, where Γ is the surface excess of the surfactant, γ is the surface tension, and μ represents the chemical potential. The advantage of molecular simulations and surface selective spectroscopies is that one can go beyond the description in terms of the integral surface excess Γ and obtain a detailed molecular picture of the distribution and orientation of the surfactants in the interfacial layer.[2-6]

Our study concerns a soluble ionic surfactant 1-dodecyl-4-dimethylaminopyridinium (DMP) bromide and a related zwitterion 2-(4-dimethylaminopyridinio)-dodecanoate (DPN) in water and in aqueous solutions of KF and KBr. The chemical structures of both species are shown in Fig. 1. These surfactants exhibit several basic features. They have both a hydrophobic moiety (carbon chain) and hydrophilic moiety (head group). Due to this asymmetric molecular structure the surfactants spontaneously self-assemble at the air/water interface, where there is an exchange of adsorbed surfactants with those in the adjacent sublayer. At the critical micelle concentration (cmc) the interface saturates and the surfactants tend to form micelles or at higher concentration more complicated structures such as vesicles or lamellas in the bulk phase.

The head groups of DMP and DPN consist of a pyridinium ring acting as an electron acceptor and a dimethylamino group acting as an electron donor. Thus, the electron density distribution creates a push-pull system resulting in a high hyperpolarizability and, consequently, in an nonlinear optical activity. On one hand, DMP has an ionic character. Once solvated the bromide anion and the cationic DMP can stay apart from each other. On the other hand, DPN is a zwitterion with the positive charge residing at the nitrogen of the pyridinium head group and the negative charge fixed at the carboxyl moiety, i.e., the separation between the charges is constrained by chemical bonds.

The present molecular dynamics (MD) simulations in a slab geometry of DMP bromide and DPN in neat water and in aqueous solutions of KF and KBr provide a detailed picture of the interface with atomic resolution, as well as thermodynamically averaged density distributions of individual species, from the surface to the bulk region. Simulations were thus carried out to explore the interfacial structures at a molecular level and to verify the interpretation of the experimental results.

The above mentioned properties of DMP and DPN enable the use of surface selective nonlinear optical techniques such as second harmonic generation (SHG) spectroscopy to characterize the structure of the interface in terms of surfactant distributions.[7] In a recent study the influence of simple salts on the adsorption behavior and the ion distribution at the interface for cationic DMP solutions with bromide as a generic counterion have been investigated by surface tension measurements, ellipsometry, and SHG spectroscopy.[6] Using an algorithm described in Refs. [5,8] ellipsometric measurements allow under certain conditions to determine the ion distribution at a charged interface. Each technique probes different structural elements and the combined data reveal a spatial distribution of bromide ions towards a condensed state at monolayer DMP coverages.

The addition of KF modifies the surface tension isotherm according to the thermodynamic Gibbs equation, but does not change the number density of adsorbed surfactants determined by SHG. Consequently, the same transition towards a condensed state of bromide anions as in the pure solution of DMP bromide was observed . However, the addition of potassium chloride or bromide leads immediately to a condensed state and strongly modifies the adsorption behaviour.[6] In the present contribution infrared-visible sum frequency generation (IR-VIS SFG) experiments of DMP bromide solutions with and without added salt have been carried out in order to observe changes in the aliphatic chain conformations and water structure at the interface. The experimental data are interpreted with the aid of the corresponding MD simulations.

Systems and Computational Methodology

An extended set of systems was prepared for the MD simulations. All these systems consist of a slab of water, varying numbers of DMP bromide or DPN surfactants and, in some cases, also additional solutes, such as KF or KBr. In detail, the following systems were investigated: water slabs with 2, 10, 20, and 40 surfactant species, and aqueous slabs containing 10 KF or KBr ion pairs together with 10 surfactants. In all cases half of the number of the surfactant species was initially placed on each of the two surfaces of the slab.

The slab geometry was realized by employing periodic boundary conditions using a prismatic box with approximate dimensions of 30 x 30 x 120 Å and 1726 water molecules in the unit cell. A polarizable force field was used. Potential parameters for potassium and halides were the same as in Refs. [9,10], for the surfactants we used the general amber force field,[11] and for water the POL3 model.[12]

The simulation protocol was as follows. A steepest descend minimization (15 000 steps) was first employed in order to remove bad contacts. This was followed by 50 ps of heating to 300 K and by a 500 ps equilibration MD run. Data were then collected from a consequent 1 ns production runs. Trajectory data were saved every 500 steps, so the production run resulted in 2000 frames used for the analysis. All MD simulations employed a time step of 1 fs. Van der Waals and electrostatic interaction were cut off at 12 Å. The long range electrostatic interactions were accounted for using the smooth particle–mesh Ewald procedure.[13] The SHAKE algorithm[14] was used to freeze all bonds connecting hydrogen atoms. Except for the heating phase, temperature was kept at 300 K and the canonical NVT ensemble was generated. All the MD simulations were carried out using the AMBER7 program package.[15]

Experimental Methods

Sample Preparation

An aqueous solution of DMP bromide close to the critical micelle concentration (cmc) of 4 mmol/L was prepared using bi-distilled water. Details about the synthesis, analysis, and various physical properties of this surfactant can be found in Ref. [16]. This solution was then purified with the aid of a fully automated device described in Ref. [17]. The purification scheme ensures the removal of any surface active impurities by repeated cycles of a) compression of the surface layer, b) its removal with the aid of a capillary, c) dilation to an increased surface area and d) again a formation of a new adsorption layer. The cleaning cycles are repeated until the equilibrium surface tension γ levels off in a plateau which indicates that all surface active trace impurities are completely removed. Solutions of different concentrations were prepared by diluting the stock solution. In order to study the impact of simple salt solutions on the adsorption behavior, we added to each solution 100 mmol/L of purified KF and KBr solutions.

Infrared-Visible Sum Frequency Generation (IR-VIS SFG)

IR-VIS SFG is a nonlinear optical technique allowing to perform surface selective optical spectroscopy with monolayer resolution.[18] In an IR-VIS SFG experiment two laser pulses are coincident in time and space at the interface of a sample. One visible laser pulse is fixed in frequency, while the other one is tunable through the infrared region of 2800 to 3800

cm^{-1}. If the intensities of the incident laser pulses are high enough they can induce a polarization of the second order in the medium which gives rise to the SFG signal traveling at the sum frequency $\omega_{SFG} = \omega_{IR} + \omega_{Vis}$ of the two incident beams.

If the frequency of the IR beam meets a vibrational mode of the interfacial molecules a resonant enhancement of the SFG signal occurs. The surface specificity is the direct consequence of a second-order nonlinear optical process. Second order processes are forbidden in media with inversion symmetry. The inversion symmetry is broken at the interface of two isotropic phases and, consequently, a SFG signal is produced within the interfacial region. Details about the theory of non-linear optics can be found in Ref. [19].

All spectra shown in this contribution are measured with a SFG spectrometer of EKSPLA. A 20-30 pico-second NdYAG laser is pumping an optical parametric generator and amplifier for tunable IR light in the region of 2800 to 3800 cm^{-1} at energies of about 200 μJ/pulse at the sample. A part of the NdYAG beam is used to pump a KTP crystal to obtain second harmonic generated green light (532 cm^{-1}) with an energy of about 1 mJ. The experiments were performed using *ssp* polarization listed in order of decreasing frequency (sum frequency, VIS, IR).

Computational Results

Snapshots and Density Profiles

Illustrative snapshots from the MD simulations and, for the more concentrated systems, also the density profiles (i.e., averaged distributions of individual species in 0.2 Å thick slices parallel with the surface) are shown in Figs. 2-7. These figures concern aqueous slabs with varying concentrations of DMP bromide or DPN with or without added salt (KF or KBr). For the single DMP or DPN species on each side of the slab the snapshots demonstrate both the inherent surfactant behavior and the varying conformations of the aliphatic chains of the isolated species (Fig. 2). All the systems involving DMP molecules exhibit similar distributions of the individual species across the slab. Namely, both the cationic DMP and the bromide anions prefer the surface region. While the surface segregation of the cationic surfactants is very strong, that of the bromide anions is much weaker, which results in a creation of a more diffuse anion distribution. This is due to the fact, that on one hand the DMP cations are “anchored” at the surface due to very strong hydrophobic forces, while on the other hand the propensity of bromide anions for the surface is due to relatively weak

polarization interactions[10,20] and, at higher concentrations, also due to surface neutralization effects.

The characteristic patterns of the density profiles of the DMP containing systems are as follows. The carbon chains, stabilized by the hydrophobic interaction, form a single peak at the air side of the slab (at and above the top-most water layer) for all concentrations. The nitrogen signal peaks closer to the aqueous phase than the carbon peak, confirming the preferential orientation of the amphiphiles with the charged head groups pointing towards the aqueous bulk and the aliphatic chain expelled from the aqueous phase. The distribution of nitrogen of the head groups gets broader and develops a shoulder towards the bulk region of the slab at higher concentrations. This indicates that upon adding more DMP surfactants a sublayer starts to build up in accordance to Refs. [21,22]. While at low concentrations the aliphatic chains of the cationic surfactants can rather freely fold and unfold at the surface, at higher concentrations the mobility of the individual chains is strongly hindered. The density profile of the bromide counterions follows the distribution of DMP nitrogens, i.e., bromide anions exhibit a density peak at the same position on the z-axis and of a similar intensity. Still, there are some bromide anions in the bulk region.

With additional salt (KF or KBr) an interesting situation arises in the slabs. In both cases, the bulk region of the slabs contains large amounts of alkali cations and halide anions. Potassium cations are always repelled from the surface. This is both due to the repulsion by the cationic surfactants and due to image charge repulsion of hard ions from the air/water interface.[23] However, the two salts differ with respect to the surface behavior of the halide anions. Fluoride, as a small non-polarizable ion is *per se* strongly repelled from the water surface.[10] Due to the attraction to the surface-bound DMP cations a very weak fluoride propensity for the sub-surface region can be observed (Fig. 6b). In the case of added KBr, there is only a single anionic species in the solution. Bromide, as a large polarizable anion, is attracted to the aqueous surface *per se*, as well as by the DMP cations. As a result, there is a sizable surface peak in the bromide distribution (see Fig. 7b). Hence, at appreciable DMP concentrations there is an increased transition of bromides towards the surface, as postulated in Refs. [24,25] using a simple thermodynamic model. This model *ad hoc* divides ions into surface-bound and bulk fractions, which is at least qualitatively correct for bromide, but not for fluoride. Interestingly, the surface adsorption of bromide is not apparent in recent Monte-Carlo simulations,[26,27] probably due to the use of a nonpolarizable force field.

The surface behavior of the DPN zwitterions is in many respects analogous to that of the cationic DMP surfactants (see Figs. 2-7). The carbon chains of DPN form again a single

peak in the top-most layer, with the nitrogen peak being somewhat broader and shifted towards the bulk phase. With rising DPN concentration a sublayer starts to form as in the DMP case. The structure of the interface is than formed by the two prevailing conformation of the DPN molecules. The DPN molecules, located in the top-most layer, prefer bent conformations with often a rather sharp angle between the carbon chain and the head group. The carboxylic moiety tends to be oriented towards the water molecules and repelled from the carbon chain. This is the preferable state from the energetic point of view and it is the only conformation that prevails for the more dilute systems. At higher concentrations, the subsurface DPN species are more straightened up with the carbon chains protruding towards the gas phase. This arrangement is apparent from the simulation snapshot depicted in the Fig. 5c.

Upon adding the KF salt (Figs. 6c,d), both potassium and fluoride reside only in the bulk region of the slab. In this respect the zwitterionic DNP is different from DMP cations – there is no preferential attraction of the anions to the surface or sub-surface due to surface neutralization. For the KBr solutions, bromide anions nevertheless exhibit a surface peak, which is due to their inherent propensity for the air/water interface (Figs. 7c,d).

Head Group Orientational Analysis

Normalized distributions of the head group orientations, defined as the angle between the N-N line and the surface normal, are shown for DMP solutions in Fig. 8 and for DPN solutions in Fig. 9. The orientation of this group has a significant importance as it is the SHG active moiety. The head group orientation exhibit an appreciable dependency on concentration. The systems involving DMP molecules show a transition from a peak in the head group orientation around 60˚ for low concentrations to 30˚ for 20 DMP. In systems with added salt orientational angles around 0˚ are also present.

The orientational angles of the DPN containing systems are as follows. The head group orientational angle peaks around 120˚ at low concentrations, while at higher concentrations and in systems with added salt a wide range of orientational angles is sampled with a preference for smaller angles (Fig. 9). The different orientational distributions compared to the systems with DMP are primarily due to the steric interaction of the carboxylic group.

Experimental Results and Comparison with Calculations

Infrared-Visible Sum Frequency Generation Measurements

The IR-VIS SFG spectra of the ionic DMP at a low concentration of 0.5 mmol/L and a concentration close to the cmc at 4 mmol/L are shown in Fig. 10 and 11. In accordance with previously discussed SHG measurements (see Fig. 12), these concentrations correspond to a number densities of 0.5 and 2.8 molecules/nm², which are directly comparable with the above simulations with 10 and 40 DMP in the unit cell.

All spectra presented in this paper have been measured under identical settings and the intensities can be directly compared. In Fig. 10 the SFG response in the spectral region from 2800 to 3000 cm^{-1} for the two different surfactant concentrations with and without addition of KBr are shown. The peaks can be attributed to CH_2 stretching modes within the aliphatic chain of the surfactant. The peak at 2850 cm^{-1} and 2915 cm^{-1} corresponds to the symmetric and asymmetric CH_2 stretch. Since the CH_2 stretching mode is not visible in an all-trans conformation of the chains due to symmetry considerations, the number of gauche defects determines the CH_2 peak intensities. A low surfactant concentration yields a significantly lower peak intensity compared to the same DMP concentration upon addition of KBr, indicating a decreased number of gauche defects in the aliphatic chain (Fig. 10a).

Each of the peak was fitted with a Lorentz oscillator and the results are shown in Table 1. The peak area of the asymmetric CH_2 stretch decreases at the low concentration by a factor of two upon adding KBr. At the higher DMP concentration of 4 mmol/L the spectra do not change significantly upon addition of KBr, neither in the peak positions nor in the peak areas. Additionally the number density of adsorbed surfactants at the cmc is the same for the pure surfactant solution and the solution where KBr was added, as shown in the next section and in Fig.12. We, therefore, conclude that the counterions were already in the condensed state prior to the addition of the salt in accordance with the MD simulations (Fig. 7) and previously done measurements.[5,22] Hence, the procedure of measuring IR-VIS SFG spectra of soluble ionic surfactants and those where counterions of the same species are added to the surfactant solution provides an experimental method to determine whether the ions are in the condensed state or not.

In Fig. 11 the IR-VIS SFG spectra in the 3000 cm^{-1} to 3600 cm^{-1} region of the DMP bromide solution with or without additional KBr are shown. Here, the intensities are

dominated by the OH-stretch of water molecules. In Fig. 11a) the spectrum of a neat water/air interface is also shown. At the ionic surfactant covered interface the IR-VIS SFG intensity is increased by a factor of 10 mainly due to an increased depth of aligned water molecules in the vicinity of a charged interface and hence, to a higher amount of oriented water molecules contributing to the IR-VIS SFG response.

The density profiles from the MD simulations in Fig. 3b, 4b and 5b indicate, that with increasing number density of adsorbed DMP the concentration of bromide ions in the interfacial region increases. At higher surface coverages almost no bromide ions reside in the center of the slab (Fig. 5). Due to this surface neutralization, the depth of aligned water molecules should be reduced with increasing amounts of bromide anions in the solution, leading to a lowered IR-VIS SFG response in the OH stretch which is indeed observed in the experiment. At the low DMP concentration the addition of KBr lowers the amount of oriented water molecules resulting in a significantly reduced IR-VIS SFG response (Fig. 11a). At the higher concentration (Fig. 11 b), where counterions are already condensed at the interface, the addition of KBr does not have a strong influence neither on the IR-VIS SFG response nor on the DMP surface coverages (as described in the next section).

In Table 2 the peak positions for water and the surfactant systems are shown. The detailed assignment of the peaks to different types of OH vibrations is still controversial[28,29] and it is not particularly relevant for the present discussion since the effects are essentially the same for all peaks. The peak positions are significantly lowered at surfactant covered interfaces and addition of KBr further decreases the peak position at each concentration. This has a different direction in comparison to IR-VIS SFG investigations of the pure water/air interface, where the addition of bromide and iodide salts leads to an increased peak in the 3400 cm^{-1} region.[30,31] Possibly, the exchange process of adsorbed surfactants with those in the bulk is playing an important role in this context and should be carefully addressed in future studies.

Second Harmonic Generation

In a recent study the adsorption behaviour of the DMP surfactant upon addition of simple salts was experimentally investigated by SHG measurements on DMP bromide in neat water and in solutions with added100 mmol/L of KBr or 100 mmol/L of KF, at DMP concentrations up to the critical micelle concentration (cmc).[6] Fig. 12 shows the corresponding number density of the surfactant headgroup as a function of surfactant bulk

concentration for the studied systems. The adsorption behaviour reveals a pronounced ion specific feature: The addition of KF practically does not change the adsorbed amount of DMP at any concentration, whereas the addition of KBr has a strong effect on the adsorption behaviour. Fluoride is not screening the charged headgoups of the adsorbed surfactants, even if the concentration of fluoride ions is 100 times higher than that of bromide ions. However, upon addition of KBr the surface charges are more screened by the increased amount of adsorbed Br ions in the vicinity of the interface which leads, consequentely, to a shift in the cmc of about one decade from 4 mmol/L to 0.5 mmol/L. The experimental results can now be interpreted with the aid of the MD simulations for 10 DMP bromides and 10 additional KF or KBr ion pairs (Figs. 6b and 7b). Whereas bromide is adsorbing at the interface, fluoride has no propensity for the surface region and, consequentely, the adsorbed amount is not increased upon addition of KF (Fig. 6b).

The SHG response stems from the surfactant headgroups due to the high hyperpolarizability of the π push-pull system of the pyridinium ring. Polarization dependent SHG measurements[7] revealed that the orientational order of the headgroup is independent of the surface coverage with a tilt angle of 59° of the long chromophore axis with respect to the surface normal and the symmetry of the molecular arrangement of the headgroup belongs to the point group $C_{\infty v}$, which is characteristic for an isotropic azimuthal arrangement within the adsorption layer. The orientation of the headgroup is in very good agreement to the MD simulations at lower surface coverages. However, the calculated change with DMP concentration is not apparent in the experiment. This might be due to the fact that the SHG response stems predominantly from the molecules in the topmost monolayer and not from the sublayer which was also included into the MD analysis.

Summary and Conclusion

Molecular dynamics simulations of ionic DMP bromide and zwitterionic DPN in aqueous slabs were performed. Both DMP and DPN strongly adsorb at the aqueous surface. At higher surface coverages a build up of a sublayer is observed. For the former system, bromide counterions mostly co-adsorb to the surface (both due to their polarizability and the presence of DMP cations) but they are also present in the bulk region. The ratio between surface adsorbed and bulk bromide anions increases with the DMP concentration up to a condensed state due to surface neutralization effects. Thus, the conventional notion of the

adsorbed Stern layer and diffuse Guy-Chapman layer naturally emerges from the MD simulations without any *ad hoc* assumptions. The effect of added salt (KF or KBr) was also investigated. On one hand, adding KF has little effect on the surface behavior of both DMP and DPN due to the fact that both potassium and fluoride strongly favor the aqueous bulk. On the other hand, added KBr affects the interface due to a significant surface propensity of bromide.

IR-VIS SFG spectroscopy has been performed on solutions of ionic DMP surfactants at various surface DMP concentrations with and without addition of KBr. The conformational changes of the aliphatic chain upon addition of KBr were monitored for a low DMP concentration and a concentration close to the cmc. Only at the low DMP concentration a significant lowering of gauche defects is observed. At the higher concentration corresponding to a condensed state for the distribution of bromide ions, the addition of salt has virtually no effect on the chain conformation. In this way one can elegantly determine the point of counterion condensation. Similarly, at low DMP concentration addition of KBr has a decreasing effect on the intensity of the OH stretching region of the spectrum, indicating an increased amount of bromide ions at the interface, while at high DMP concentrations the change is small.

The results of the present MD simulations support the above conclusions as well as the results of previous SHG and ellipsometry measurements in a series of potassium halides solutions. In particular, MD simulations provide rationalization for the strong effect of added KBr and the lack of effect for added KF in terms of different surface behavior of bromide versus fluoride. Furthermore the experimentally observed condensed state for bromide at higher surface DMP coverages was reproduced in the MD simulations.

Acknowledgment

Support from the Granting Agency of the Academy of Sciences (grant IAA400400503), the Czech Ministry of Education (grant LC512), and the NSF (grants CHE 0209719 and 0431312) is gratefully acknowledged. L.V. and B. M. would like to thank the Granting Agency of the Czech Republic for support (grant 203/05/H001). P.K. and H.M. thank Prof. Möhwald for his steady support and stimulating discussions.

Figure captions

Figure 1: a) Chemical structure of a) DMP and b) DPN.

Figure 2: Snapshot from a MD simulation of an aqueous slab with a) 2 DMP and b) 2 DPN.

Figure 3: a) Snapshot from a MD simulation of an aqueous slab with 10 DMP and b) the corresponding density profiles. c) Snapshot from a MD simulation of an aqueous slab with 10 DPN and d) the corresponding density profiles.

Figure 4: a) Snapshot from a MD simulation of an aqueous slab with 20 DMP and b) the corresponding density profiles. c) Snapshot from a MD simulation of an aqueous slab with 20 DPN and d) the corresponding density profiles.

Figure 5: a) Snapshot from a MD simulation of an aqueous slab with 40 DMP and b) the corresponding density profiles. c) Snapshot from a MD simulation of an aqueous slab with 40 DPN and d) the corresponding density profiles.

Figure 6: a) Snapshot from a MD simulation of an aqueous slab with 10 DMPs and 10 additional KF ion pairs and b) the corresponding density profiles. c) Snapshot from a MD simulation of an aqueous slab with 10 DPNs and 10 additional KF ion pairs and d) the corresponding density profiles.

Figure 7: a) Snapshot from a MD simulation of an aqueous slab with 10 DMPs and 10 additional KBr ion piars and b) the corresponding density profiles. c) Snapshot from a MD simulation of an aqueous slab with 10 DPNs and 10 additional KBr ion pairs and d) the corresponding density profiles.

Figure 8: Head group orientation for a) 2 DMP, b) 10 DMP, c) 40 DMP, d) 10 DMP and 10 additional KF ion pairs, and e) 10 DMP and 10 additional KBr ion pairs.

Figure 9: Head group orientation for a) 2 DPN, b) 10 DPN, c) 40 DPN, d) 10 DPN and 10 additional KF ion pairs, and e) 10 DPNs and 10 additional KBr ion pairs.

Figure 10: IR-VIS SFG spectra in the region of 2800 cm^{-1} to 3000 cm^{-1} at different surfactant concentrations with (filled) and without (blank) addition of 100 mmol/L KBr. a) 0.5 mmol/L DMP bromide, and b) 4.0 mmol/L DMP bromide. All spectra were measured in SSP configuration.

Figure 11: IR-VIS SFG spectra in the region of 3000 cm^{-1} to 3600 cm^{-1} at different surfactant concentrations with (filled) and without (blank) addition of 100 mmol/L KBr. a) 0.5 mmol/L DMP bromide, and b) 4.0 mmol/L DMP. In a) the neat water/air spectrum is shown as well. All spectra were measured in SSP configuration.

Figure 12: Number density of the adsorbed surfactant headgroup at the interface as a function of concentration for DMP solutions and where 100 mmol/L KF and KBr are added to the DMP bromide solution.[6]

Table 1: Average frequencies and peak areas for the resonant peaks of DMP and DMP plus addition of salt with their corresponding uncertainties in the CH stretch.

Table 2: Average frequencies for the resonant peaks of DMPB and DMPB plus addition of salt with their corresponding uncertainties in the OH stretch.

Figure 1:

a)

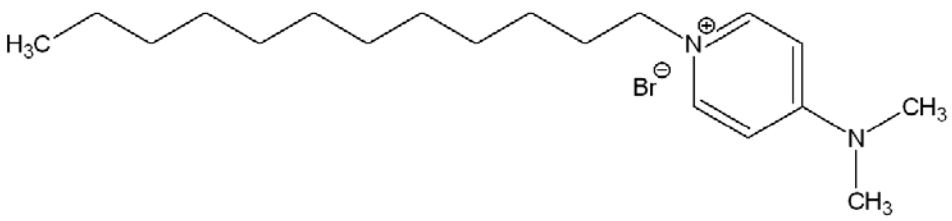

b)

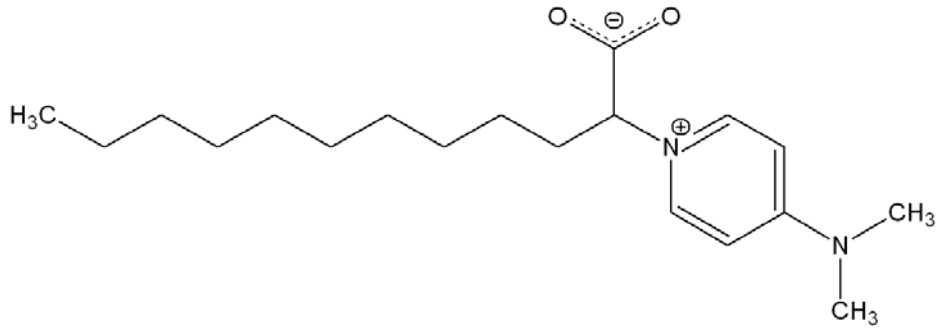

Figure 2:

a) **b)**

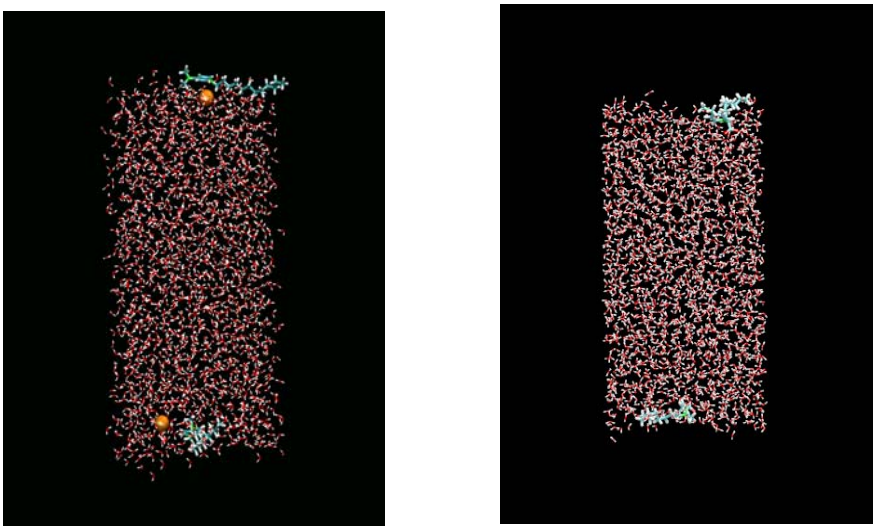

Figure 3:

a)

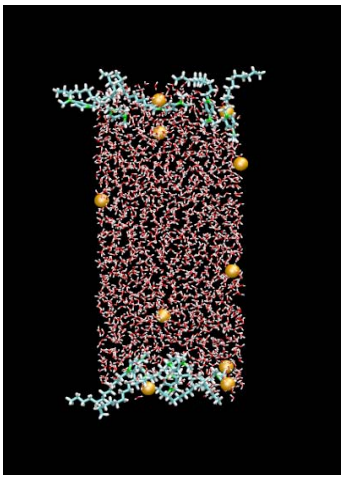

b)

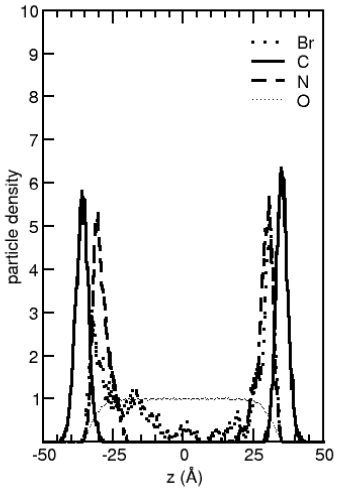

c)

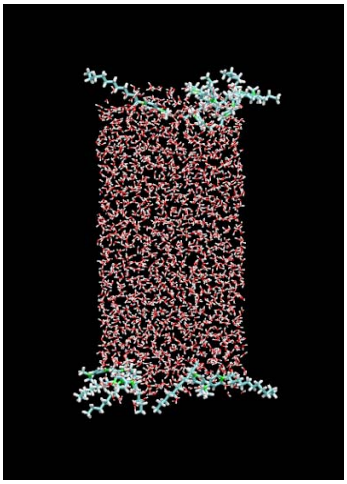

d)

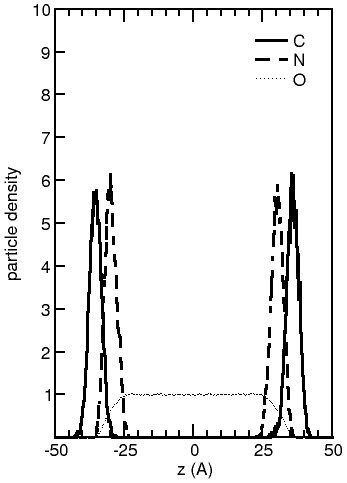

Figure 4:

a)

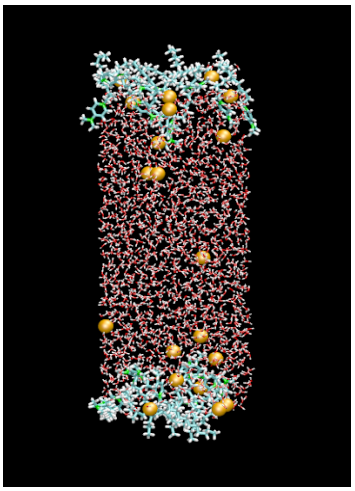

b)

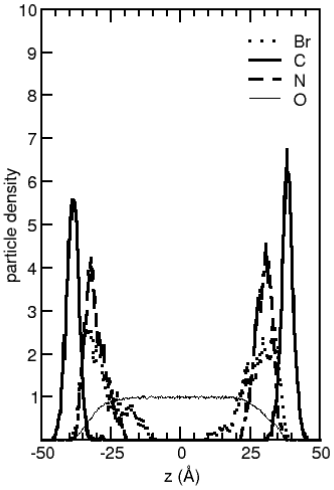

c)

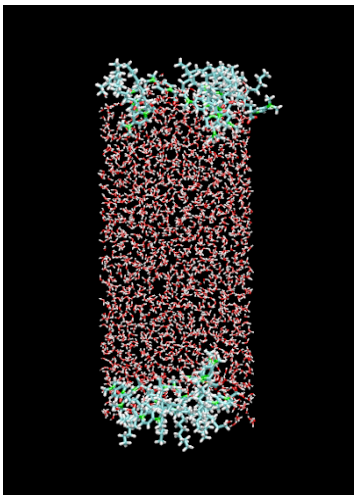

d)

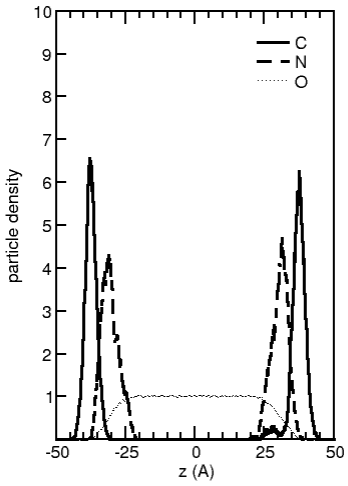

Figure 5:

a)

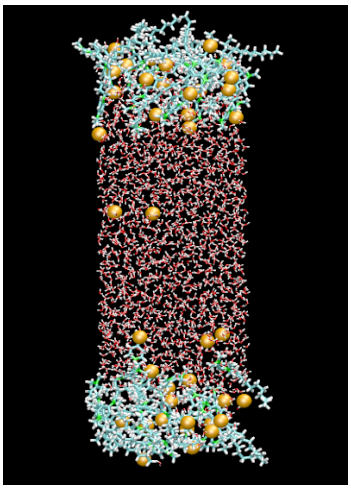

b)

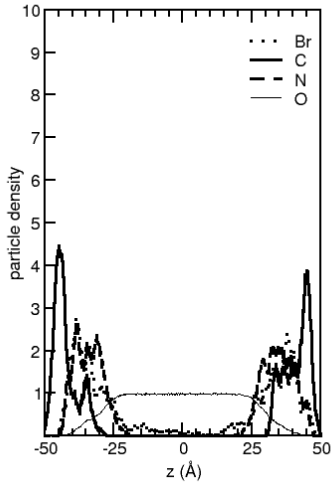

c)

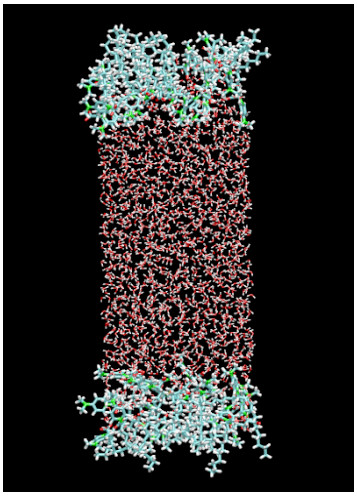

d)

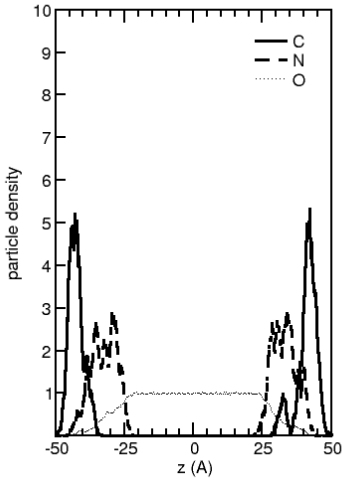

Figure 6:

a)

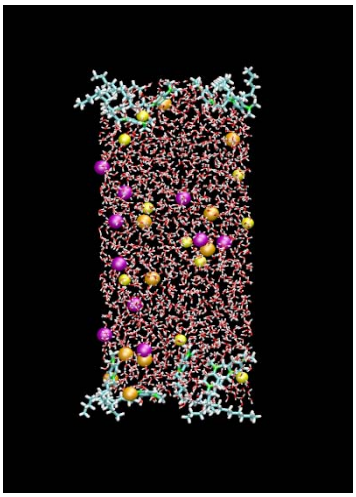

b)

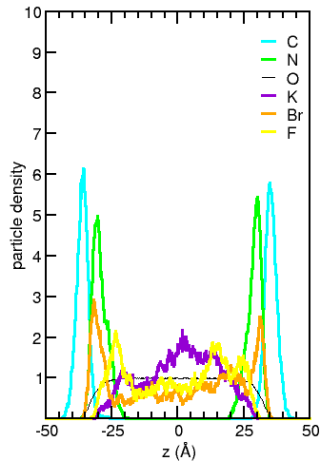

c)

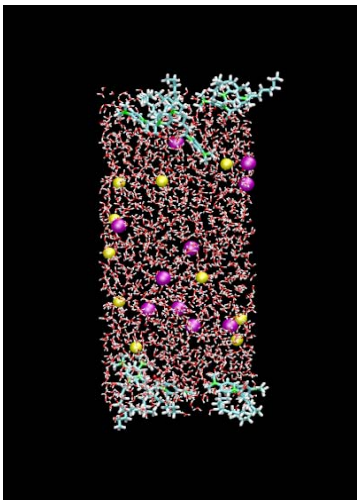

d)

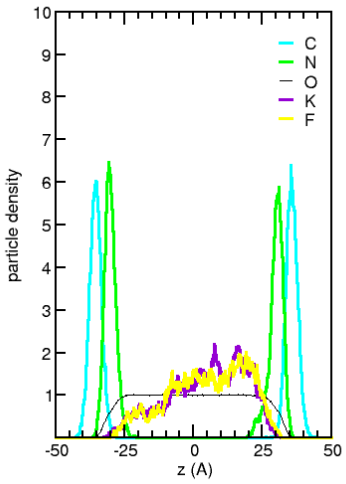

Figure 7:

a)

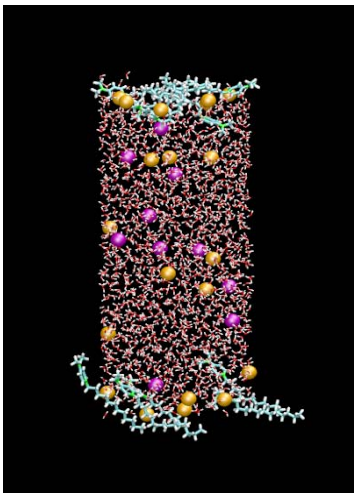

b)

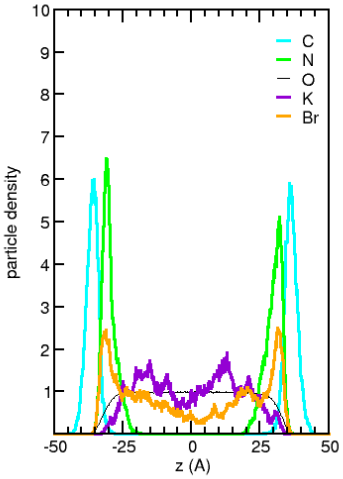

c)

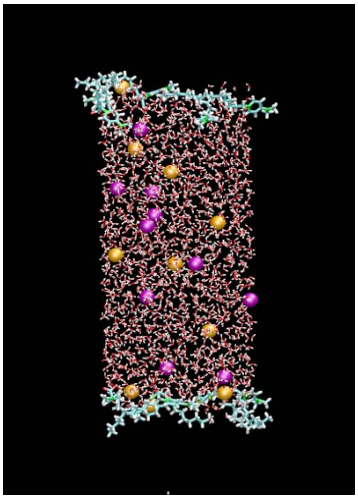

d)

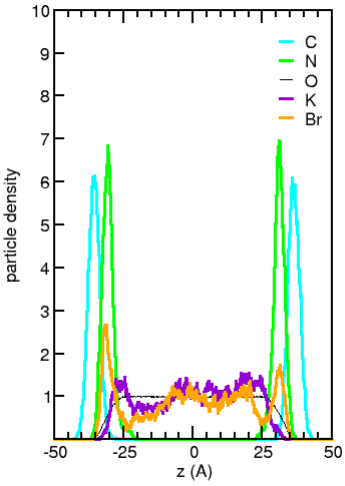

Figure 8:

a) **b)** **c)**

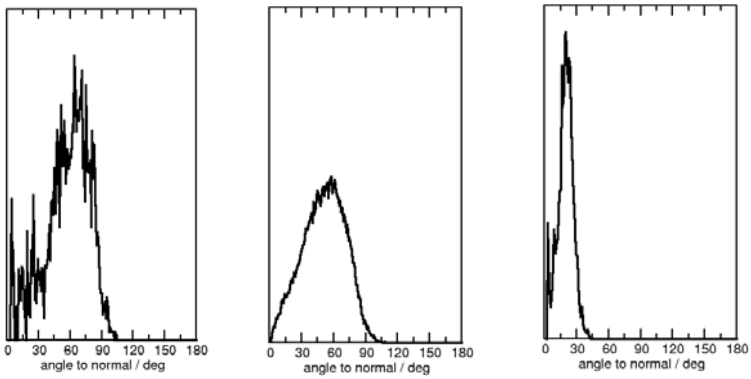

d) **e)**

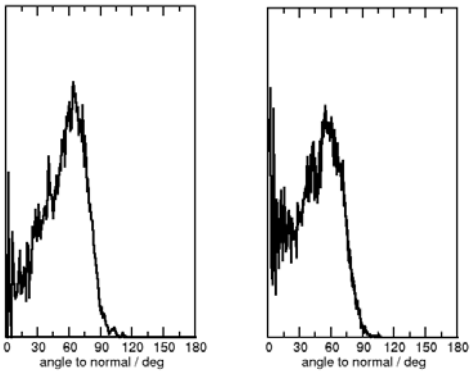

Figure 9:

a) **b)** **c)**

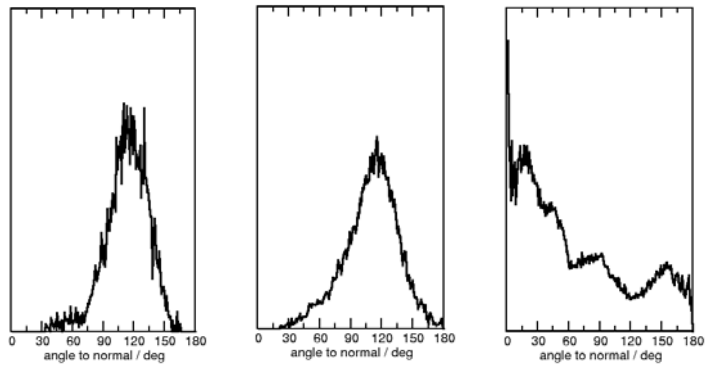

d) **e)**

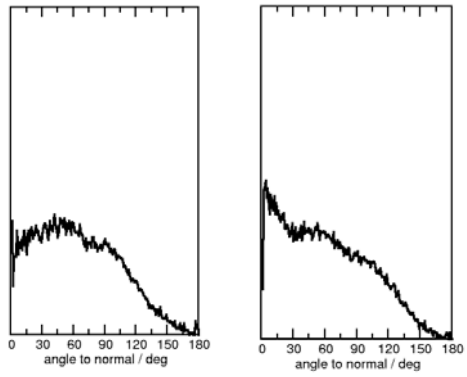

Figure 10:

a) **b)**

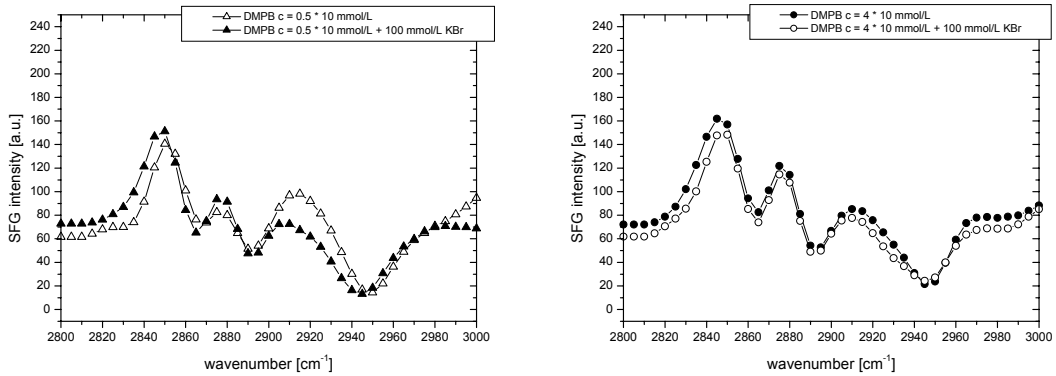
DMPB c = 0.5 * 10 mmol/L
DMPB c = 0.5 * 10 mmol/L + 100 mmol/L KBr
SFG intensity [a.u.]
wavenumber [cm-1]
DMPB c = 4 * 10 mmol/L
DMPB c = 4 * 10 mmol/L + 100 mmol/L KBr
SFG intensity [a.u.]
wavenumber [cm-1]

Figure 11:

a)

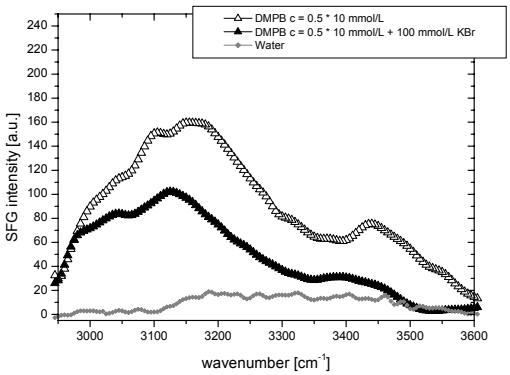
DMPB c = 0.5 * 10 mmol/L
DMPB c = 0.5 * 10 mmol/L + 100 mmol/L KBr
Water
SFG intensity [a.u.]
wavenumber [cm-1]

b)

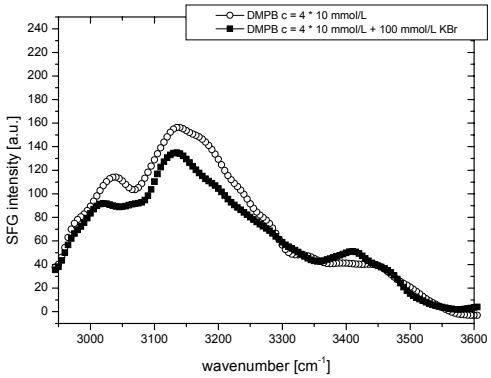
DMPB c = 4 * 10 mmol/L
DMPB c = 4 * 10 mmol/L + 100 mmol/L KBr
SFG intensity [a.u.]
wavenumber [cm-1]

Figure 12:

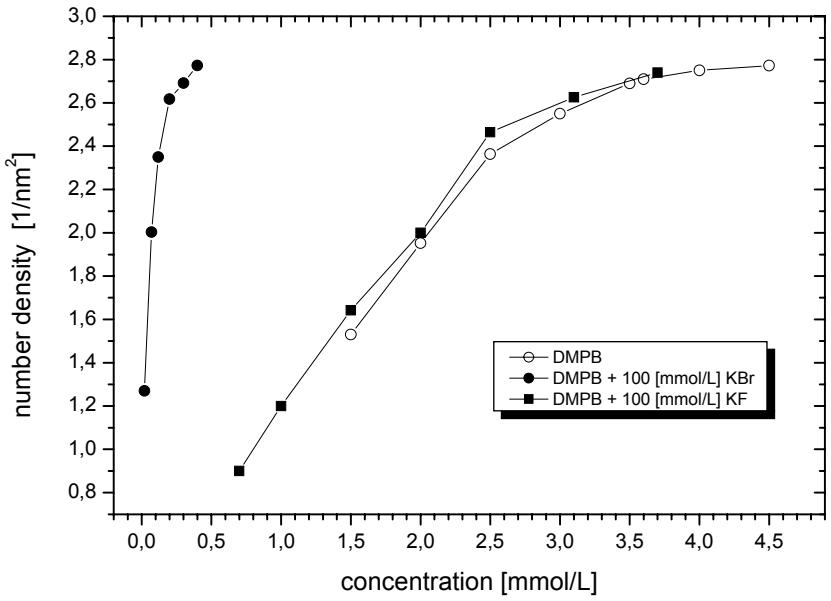
number density [1/nm²]
concentration [mmol/L]
DMPB
DMPB + 100 [mmol/L] KBr
DMPB + 100 [mmol/L] KF

Table 1:

	symmetric CH_2 stretch		symmetric CH_3 stretch		asymmetric CH_2 stretch	
	wavenumber	**Area/100**	**wavenumber**	**Area/100**	**wavenumber**	**Area/100**
DMP 0.5 mmol/L	2851.1 ± 0.4	2.5 ± 0.2	2877.5 ± 0.6	0.30 ± 0.07	2918.3 ± 0.6	4.7 ± 0.4
DMP 0.5 mmol/L + 100 mmol/L KBr	2847.5 ± 0.5	2.7 ± 0.3	2877.9 ± 0.6	0.4 ± 0.1	2915.4 ± 1.4	2.0 ± 0.4
DMP 4 mmol/L	2845.6 ± 0.6	4.0 ± 0.4	2877.3 ± 0.4	0.9 ± 0.2	2918.5 ± 1.2	3.5 ± 0.6
DMP 4 mmol/L + 100 mmol/L KBr	2846.9 ± 0.6	3.1 ± 0.4	2877.4 ± 0.5	0.9 ± 0.2	2917.7 ± 1,6	3.6 ± 0.7

Table 2:

	wavenumber	**wavenumber**	**wavenumber**
Water	3190 ± 3	3306 ± 6	3459 ± 5
DMP 0.5 mmol/L	3178 ± 5	3277 ± 18	3454 ± 2
DMP 0.5 mmol/L + 100 mmol/L KBr	3127 ± 3	3229 ± 14	3407 ± 3
DMP 4 mmol/L	3145 ± 3	3246 ± 10	3428 ± 3
DMP 4 mmol/L + 100 mmol/L KBr	3135 ± 2	3243 ± 7	3417 ± 2

TOC:

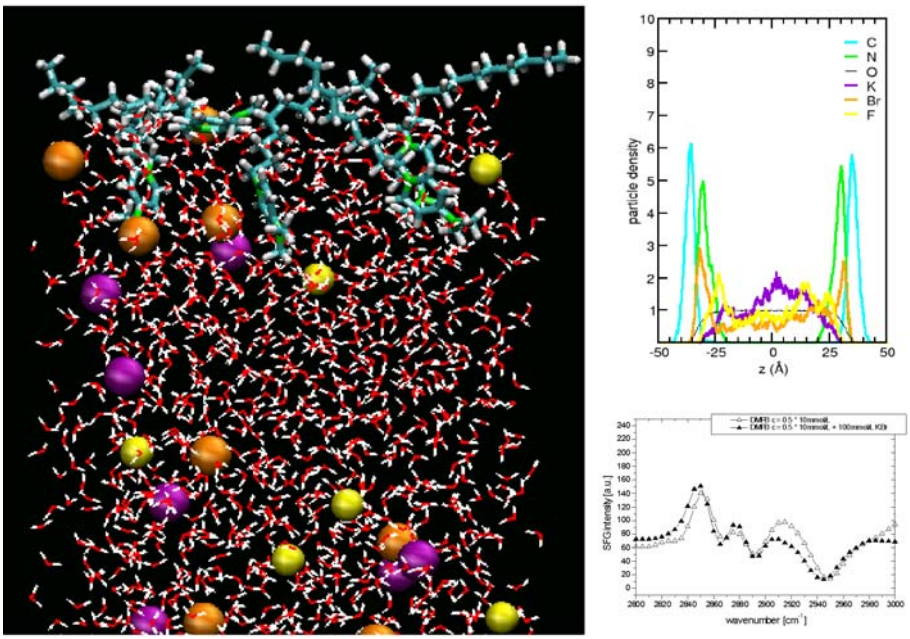
C
N
O
K
Br
F
particle density
z (Å)
SFGintensity [a.u.]
wavenumber [cm⁻¹]

References:

(1) Adam, N. K. *The Physics and Chemistry of Surfaces*; Oxford University Press: London, 1941.

(2) Dukhin, S. S.; Kretzschmar, G.; Miller, R. *Dynamics of Adsorption at Liquid Interfaces - Theory, Experiment, Application*; Elsevier: Amsterdam, 1995.

(3) Tarek, M.; Tobias, D. J.; Klein, M. L. *Journal of Physical Chemistry* **1995**, *99*, 1393.

(4) Winter, B.; Weber, R.; Schmidt, P. M.; Hertel, I. V.; Faubel, M.; Vrbka, L.; Jungwirth, P. *Journal of Physical Chemistry B* **2004**, *108*, 14558.

(5) Koelsch, P.; Motschmann, H. *Journal of Physical Chemistry B* **2004**, *108*, 18659.

(6) Koelsch, P.; Motschmann, H. *Langmuir* **2005**, *21*, 3436.

(7) Bae, S.; Haage, K.; Wantke, K.; Motschmann, H. *Journal of Physical Chemistry B* **1999**, *103*, 1045.

(8) Koelsch, P.; Motschmann, H. *Current Opinion in Colloid & Interface Science* **2004**, *9*, 87.

(9) Chang, T. M.; Dang, L. X. *Journal of Physical Chemistry B* **1999**, *103*, 4714.

(10) Jungwirth, P.; Tobias, D. J. *Journal of Physical Chemistry B* **2001**, *105*, 10468.

(11) Wang, J. M.; Wolf, R. M.; Caldwell, J. W.; Kollman, P. A.; Case, D. A. *Journal of Computational Chemistry* **2004**, *25*, 1157.

(12) Caldwell, J. W.; Kollman, P. A. *Journal of Physical Chemistry* **1995**, *99*, 6208.

(13) Essmann, U.; Perera, L.; Berkowitz, M. L.; Darden, T.; Lee, H.; Pedersen, L. G. *Journal of Chemical Physics* **1995**, *103*, 8577.

(14) Ryckaert, J.-P.; Ciccotti, G.; Berendsen, H. J. C. *Journal of Computational Physics* **1977**, *23*, 327.

(15) Case, D. A. P., D.A.; Caldwell, J.W.; Cheatham III, T.E.; Wang, J.; Ross, W.S.; Simmerling, C.L.; Darden, T.A.; Merz, K.M.; Stanton, R.V.; Cheng, A.L.; Vincent, J.J.; Crowley, M.; Tsui,V.; Gohlke, H.; Radmer, R.J.; Duan, Y.; Pitera, J.; Massova, I.; Seibel, G.L.; Singh, U.C.; Weiner, P.K.; Kollman, P.A. Amber7; Amber7, University of California: San Francisco, 2002.

(16) Haage, K.; Motschmann, H.; Bae, S. M.; Grundemann, E. *Colloids and Surfaces a-Physicochemical and Engineering Aspects* **2001**, *183*, 583.

(17) Lunkenheimer, K.; Pergande, H. J.; Kruger, H. *Review of Scientific Instruments* **1987**, *58*, 2313.

(18) Shen, Y. R. *Annual Review of Physical Chemistry* **1989**, *40*, 327.

(19) Shen, Y. R. *The Principles of Nonlinear Optics*; Wiley: New York, 1984.

(20) Jungwirth, P.; Tobias, D. J. *Journal of Physical Chemistry B* **2002**, *106*, 6361.

(21) Ortegren, J.; Wantke, K. D.; Motschmann, H.; Mohwald, H. *Journal of Colloid and Interface Science* **2004**, *279*, 266.

(22) Koelsch, P.; Motschmann, H. *Langmuir* **2005**, *21*, 6265.

(23) Onsager, L.; Samaras, N. N. T. *Jornal of Chemical Physics* **1934**, *2*, 528.

(24) Lau, A. W. C.; Pincus, P. *Physical Review E* **2002**, *66*.

(25) Lau, A. W. C.; Lukatsky, D. B.; Pincus, P.; Safran, S. A. *Physical Review E* **2002**, *65*.

(26) Moreira, A. G.; Netz, R. R. *European Physical Journal E* **2002**, *8*, 33.

(27) Netz, R. R.; Orland, H. *European Physical Journal E* **2000**, *1*, 203.

(28) Richmond, G. L. *Chemical Reviews* **2002**, *102*, 2693.

(29) Buch, V. *Journal of Physical Chemistry B* **2005**, *109*, 17771.

(30) Liu, D. F.; Ma, G.; Levering, L. M.; Allen, H. C. *Journal of Physical Chemistry B* **2004**, *108*, 2252.

(31) Raymond, E. A.; Richmond, G. L. *Journal of Physical Chemistry B* **2004**, *108*, 5051.